Microchim Acta 155, 305–311 (2006)
DOI 10.1007/s00604-006-0561-6

Microchimica Acta
Printed in Austria

Original Paper

Micro-PIXE Analysis of Monazite from the Dora Maira Massif, Western Italian Alps**

Gloria Vaggelli[1,*], **Alessandro Borghi**[1,2], **Roberto Cossio**[2,3], **Mariaelena Fedi**[4], **Lorenzo Giuntini**[4], **Bruno Lombardo**[1], **Aldo Marino**[5], **Mirko Massi**[4], **Filippo Olmi**[6], and **Maurizio Petrelli**[7]

[1] CNR – Istituto di Geoscienze e Georisorse, Via V. Caluso 35, Torino, Italy
[2] Dipartimento di Scienze Mineralogiche e Petrologiche, Università degli Studi di Torino, Via V. Caluso 35, Torino, Italy
[3] Dipartimento di Fisica Sperimentale, Via P. Giuria 1, Torino, Italy
[4] Dipartimento di Fisica – INFN Firenze, via Sansone 1, Sesto Fiorentino, Italy
[5] Paschera San Carlo 66 bis, Caraglio, Italy
[6] CNR – Istituto di Geoscienze e Georisorse, Via G. La Pira 4, I-50121 Firenze, Italy
[7] Dipartimento di Scienze della Terra, Piazza dell'Università 1, Perugia, Italy

Received May 26, 2005; accepted November 26, 2005; published online April 18, 2006

Abstract. Quantitative micro-PIXE and electron microprobe analyses, as well as micro-PIXE compositional mapping of trace elements were performed on monazite [(Ce, La, Nd, Th)PO_4] inclusions in pyrope megablasts from Dora Maira Massif, Western Italian Alps for petrological and geochronological purposes.

Monazite was studied by SEM-BSE imaging and by X-ray qualitative compositional maps of major elements; further WDS electron microprobe analyses were carried out in areas showing different BSE intensity in order to quantify chemical zoning. Finally, micro-PIXE compositional maps and quantitative analyses were performed on selected spots and areas. EPMA data indicate that the Dora Maira monazite is Ce- and Th-rich with homogeneous concentrations of LREE, but with a significantly heterogeneous distribution of Th, as well as of Y, Sr, U and Pb as displayed by micro-PIXE compositional mapping. HREE mostly occur in concentrations below the detection limit for standard quantitative EPMA. Th–U–Pb zoning suggests two monazite growth events, dated at 35 (±7 Ma) and 60 Ma (±10 Ma), respectively. While the younger age of 35 Ma found in high-Th monazite areas corresponds to the thermal and baric peak of the UHP metamorphism in the Dora Maira Massif, in agreement with previous literature data, the older ages of 60 Ma found in low-Th areas have to be confirmed by U–Th–Pb isotopic data.

Key words: Monazite; Western Alps; EPMA; micro-PIXE; U–Th–Pb ages.

Monazite is a rare earth element (REE) phosphate mineral [(Ce, La, Nd, Th, Y) PO_4] that is present as an accessory mineral phase in many igneous and metamorphic rocks.

Monazite is commonly rich in Th and U and extremely poor in non-radiogenic Pb. Also, because diffusion of trace components is extremely slow, monazite has the potential to retain chemical and geochronological information through multiple metamorphic events [1].

Consequently the simultaneous and precise determination of U, Th and Pb allows one to determine a geological age corresponding to the time of monazite growth. Indeed, assuming that the amount of common Pb and Pb diffusion in monazite are negligible, the measured Pb can be derived only by Th and U decay.

* Author for correspondence. E-mail: vaggelli@igg.cnr.it
** The authors dedicate this paper to the memory of co-author Filippo Olmi who has left us after the article had been submitted

Modelling the U and Th decay allows the age of monazite to be measured using an analytical system such as electron microprobe (EPMA) for old (>100 Ma) monazite where Pb occurs in concentrations above the EPMA minimum detection limit (MDL), or using micro-PIXE (i.e. an analytical system with a lower MDL for Pb) for younger monazites.

The chemical dating method proposed by [2, 3] was developed using U–Th–Pb EPMA data on monazite older that 100 Ma. Indeed, the youngest age that can be measured is directly related to the MDL for Pb that for standard EPMA working conditions is around 200 ppm. Micro-PIXE facility combines the capability of high sensitivity (MDL much lower relative to EPMA) with a high spatial resolution. In addition, its mapping abilities give much information on the U–Th–Pb behaviour in monazite at the crystal scale [4], making it possible to produce age maps of single crystals.

Examples of monazite dating by micro-PIXE are reported in [5, 6]. Both studies concern old monazite, but whereas [6] compare the micro-PIXE results with EPMA data, in [5] the matrix concentration of monazite is estimated only by the GUPIX routine for matrix iteration and was not measured by an independent system such as EPMA.

Here we present the results of a combined study by EPMA and micro-PIXE on young (i.e. <100 Ma) monazite crystals occurring in the Dora Maira Massif, Western Alps, Italy. The EPMA data were collected both for a chemical and petrological characterisation of the studied monazites, and for the matrix and density calculations necessary for processing the micro-PIXE spectra.

Experimental

Preparation, Description and Selection of Monazite Samples

The studied monazite crystals were found as mineral inclusions in pyrope megablasts from the pyrope-bearing whiteschists occurring within the granitic orthogneiss of the Ultra High Pressure (UHP) Brossasco-Isasca Unit of the Dora Maira Massif, Western Alps [7]. The pyrope-bearing whiteschists mainly consist of pyrope megablasts (from a few mm up to 20 cm in size) embedded in a matrix composed of quartz, phengite, talc and kyanite. The pyrope megablasts have inclusions of coesite, kyanite and accessory minerals such as rutile, coesite, zircon, monazite, ellenbergerite and fosfo-ellenbergerite, talc, clinochlore and very rarely magnesio-dumortierite and magnesio-staurolite [8]. The pyrope megablasts with the monazite inclusions analysed here were sampled in the outcrop of Case Tapina, left side of Vallone Gilba, Brossasco, Provincia di Cuneo, Italy.

An optical stereoscopic microscope was firstly used for locating monazite occurring both inside and on the border of the pyrope megablasts. Five thick polished sections, such as for conventional electron microprobe analysis, were prepared. Monazite occurs both as single crystals 100–500 μm long (samples MLM3B and MLM4) and as aggregates of several crystals 500 μm–1 mm in size (samples MLM2 and MLM3A) (Fig. 1A). Scanning electron microscope imaging (SEM-BSE) and X-ray mapping (SEM-EDS) were carried out in order to check sample homogeneity and to detect evidence for chemical zoning of major elements (Fig. 1B). Electron microprobe analyses were performed on several monazite crystals occurring in four different pyrope megablasts. Finally, micro-PIXE chemical analyses and X-ray quantitative mapping were performed in order to measure U–Th–Pb concentrations on 3 single monazite crystals (MLM2, MLM3a, MLM3b) and quantify element zoning.

WDS Microprobe Analysis

WDS electron microprobe analyses were performed with a JEOL JXA 8600 superprobe at 15 kV and 200 nA of probe current. As for any high-precision analysis long counting times and high sample currents are necessary. REE were detected using Lα or Lβ X-ray lines. P, Si, Ca, and F were detected using Kα; Th and Pb were detected with Mα and U with Mβ X-ray lines according to [3]. Different counting times were selected: 10 sec for major elements

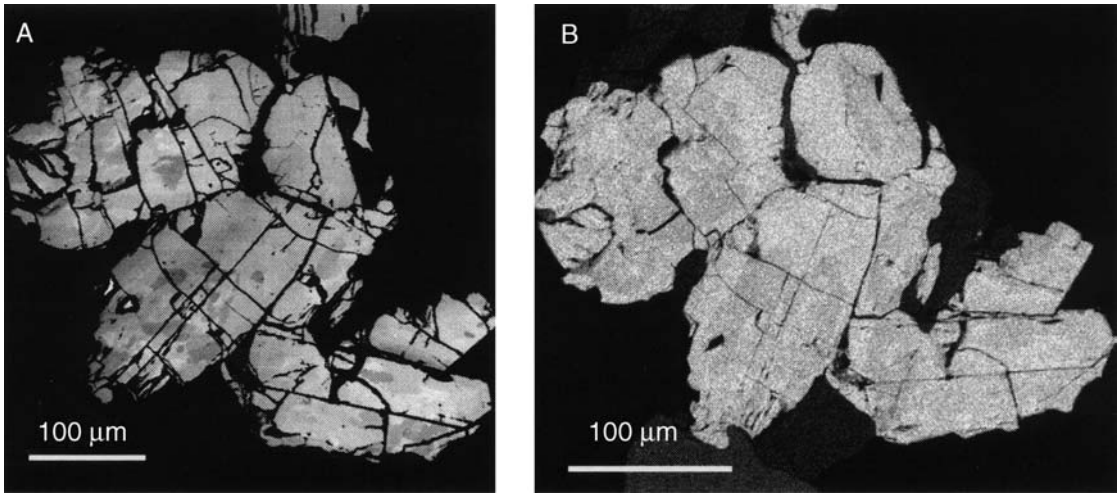

Fig. 1. (A) S.E.M. backscattered electron image of MLM3A monazite. (B) Qualitative X-ray compositional map of Th in MLM3A monazite

such as P, La and Ce; 30 sec for LREE, HREE, Si, Ca, F, Sr and Y; 50 sec for U, Th and Pb. Synthetic REE phosphates [9], pure elements and natural minerals were used as primary standards. A ZAF matrix correction routine was applied. According to the chosen analytical condition the MDL for REE varies from 400 to 800 ppm and it is about 250 ppm for U, Th and Pb.

Micro-PIXE Facility

During 2004 the installation of the external proton microprobe facility, on a beam line of the new 3 MV Tandetron accelerator at the LABEC laboratory of INFN in Florence, was completed. The facility is now available for compositional investigation of samples through Ion Beam Analysis.

An optical aiming system, via a micro camera displaying an area of about 1 mm^2 on a TV screen, allows fast identification of the detail to be analysed.

The facility is equipped with a combined beam-scanning and sample-movement system which altogether allows real time collection of elemental maps for all detected elements, over any user-defined area within a scan size up to $25 \times 25\ mm^2$. The detection setup is arranged to perform PIXE (Particle Induced X-ray Emission), BS (Backscattering Spectroscopy) and PIGE (Particle Induced Gamma-ray Emission) measurements. For micro-PIXE analyses the detection system is based on two energy dispersive detectors: Si(Li) and Ge. The Si(Li) spectrometer (named SMALL) is dedicated to lower energy X-rays, whereas the Ge spectrometer (named BIG) is used for higher energy X-rays.

An essential feature of the system is the possibility of acquiring data in list mode and to reprocess them off-line, e.g. focusing the analysis to a particular area of the sample, and/or gating on spectrum intervals related to elements or background.

In order to have a good sensitivity for heavy elements, such as U, Th and Pb, high beam currents were used. Since in these measurements the maximum spatial resolution was not required, we slightly

Table 1. Representative WDS electron microprobe analyses of the Tapina monazite expressed as wt.% and atoms per formula unit based on 4 oxygens. For each sample, spot analyses of the high- and low Th areas are given

Sample	MLM2	MLM2	MLM3A	MLM3A	MLM3B	MLM3B	MLM4	MLM4
P_2O_5	28.77	28.71	28.73	27.55	27.25	27.12	27.07	26.21
Ce_2O_3	26.93	29.38	27.00	28.84	27.57	28.77	26.37	28.00
La_2O_3	12.31	11.75	12.67	13.25	11.17	10.96	10.54	10.89
Nd_2O_3	11.53	11.91	10.17	11.78	10.21	11.20	10.49	10.74
Pr_2O_3	5.11	5.04	4.57	5.16	4.45	4.78	4.95	5.19
Sm_2O_3	2.21	1.90	1.67	1.99	1.81	1.95	1.99	1.94
Gd_2O_3	1.01	0.88	1.10	0.86	0.89	0.91	0.96	0.84
ThO_2	10.06	7.43	10.52	7.57	9.46	7.25	9.59	7.94
PbO	bdl	bdl	bdl	bdl	bdl	bdl	bdl	bdl
SrO	n.a.	n.a.	n.a.	n.a.	0.31	0.36	0.33	0.41
CaO	1.83	1.48	1.74	0.88	1.37	0.87	1.53	0.91
Eu_2O_3	0.08	0.11	0.01	0.07	bdl	0.08	0.10	bdl
Dy_2O_3	0.16	0.06	0.16	bdl	0.13	0.04	0.13	bdl
Y_2O_3	0.26	0.14	0.41	0.04	0.24	0.03	0.03	0.06
Tb_2O_3	0.03	0.06	0.04	0.06	bdl	bdl	bdl	0.11
Yb_2O_3	bdl	bdl	bdl	bdl	bdl	bdl	bdl	bdl
Er_2O_3	0.03	0.08	0.06	bdl	bdl	bdl	bdl	bdl
SiO_2	0.01	bdl	0.36	0.45	0.94	1.37	0.34	0.58
F	0.24	0.26	0.32	0.21	0.25	0.33	0.28	0.25
Total	100.57	99.19	99.53	98.71	96.05	96.02	94.70	94.07
P	1.013	1.011	1.012	0.970	0.960	0.955	0.954	0.923
Si	0.000	0.000	0.014	0.018	0.039	0.056	0.014	0.025
La	0.180	0.174	0.186	0.200	0.170	0.166	0.163	0.172
Ce	0.392	0.431	0.393	0.431	0.417	0.433	0.406	0.439
Pr	0.074	0.074	0.066	0.077	0.067	0.072	0.076	0.081
Nd	0.164	0.171	0.145	0.172	0.151	0.165	0.158	0.164
Sm	0.030	0.026	0.023	0.028	0.026	0.028	0.029	0.029
Eu	0.001	0.002	0.000	0.001	0.000	0.001	0.001	0.000
Gd	0.013	0.012	0.015	0.012	0.012	0.012	0.013	0.012
Tb	0.000	0.001	0.001	0.001	0.000	0.000	0.000	0.002
Dy	0.002	0.001	0.002	0.000	0.002	0.001	0.002	0.000
Er	0.000	0.001	0.001	0.000	0.000	0.000	0.000	0.000
Yb	0.000	0.000	0.000	0.000	0.000	0.000	0.000	0.000
Ca	0.078	0.064	0.074	0.039	0.061	0.038	0.069	0.042
Y	0.005	0.003	0.009	0.001	0.005	0.001	0.001	0.001
Th	0.091	0.068	0.095	0.070	0.089	0.068	0.092	0.077
Sum cations	2.046	2.037	2.036	2.020	1.997	1.996	1.978	1.966
F	0.030	0.033	0.040	0.027	0.033	0.043	0.037	0.034

bdl Below detection limit; *n.a.* not analyzed.

opened the collimation and object slit apertures in order to increase the beam current on the target. We could not increase the initial beam current more than ~3 μA due to the problem of radiation safety. Beam characteristics for these measurements were proton energy of ~3 MeV with a current of 2–3 nA on the target (which was placed 2 mm out of the exit window), He flow and a spot size of ~20 μm FWHM.

In this condition of higher beam current, in order to limit on the detectors the count rate of X-rays produced by elements of medium to low atomic number, such as the REE (high production cross sections of L-series X-rays), present in large abundance in monazite, we reduced the solid angle of the SMALL spectrometer with a collimator and the X-ray transmission to the BIG spectrometer with an absorber layer. Good measurement conditions came out to be a SMALL solid angle of 0.1 msr and an absorber layer for the BIG made of Mylar foils with an overall thickness of 620 μm + Al foils for an overall 25 μm thickness. The detectors were positioned at ~135° to the beam. With the beam current monitoring system described above we measured the beam current with a Si X-ray yield of ~700 counts per nC.

The acquisition times for PIXE spectra were depending on the scanned area. For spot analyses (i.e. small scanned areas of 50 μm × 50 μm) a time of 30 min was sufficient for achieving a good peak/background ratio. For mapping areas (i.e. 50 × 1 mm) a dwell time of 90 min was necessary at counts rate of about 2000 cps.

Micro-PIXE spectra were finally processed by the GUPIX software package [10, 11]. The matrix composition and density were calculated using the corresponding electron microprobe analyses on monazite. MDL of 100, 80 and 60 ppm were achieved for U, Th and Pb, respectively.

Results and Discussion

Microchemical study of monazite from the Case Tapina outcrop showed in several crystals a patchy zoning characterised by irregular interlocking zones with variable compositions (Fig. 1A). The same type of zoning was noted by [8] on back-scattered electron images of the Case Ramello (Parigi) monazite crystals. Compositional data on an aggregate of crystals (sample MLM3A) are here reported in order to summarize all the main features. X-ray qualitative maps of major elements (i.e. LREE) do not show an evident chemical zoning. However, Th displays a rough but sharp and significant increase from core to rim of most crystals (Fig. 1B). Th chemical changes are not perfectly regular as some areas show ''patchy'' zoning with spots of either high or low Th contents.

Major-element composition of monazite was determined by WDS-EPMA, while trace elements and the U and Pb concentrations were measured by micro-PIXE.

A representative set of EPMA data are reported in Table 1. Quantitative spot analyses indicate that the Tapina monazite is Ce-rich, with ThO_2 contents ranging from about 7 wt.% to nearly 11 wt.% and showing sharp and irregular changes. Variations in Th concentration are accompanied by an increase of some minor elements such as Ca and Sr and by changes in concentration of some of the LREE (Ce_2O_3: 26 ÷ 30 wt.%; La_2O_3: 10.5 ÷ 13.5 wt.%; Nd_2O_3: 10.5 ÷ 12 wt.%). U and Pb concentrations range between 500 and 2000 ppm, and from 100 to 250 ppm, respectively. Y is present at the thousand ppm level.

Th enrichments suggest the development of a cheralite phase which is a solid solution intermediate between the two end-members Ce-monazite ($CePO_4$) and brabantite ($CaThPO_4$) which have complete miscibility [12]. The cheralite phase seems to have developed at the expenses of an earlier, less Th-rich (Ce)-monazite suggesting the occurrence of two monazite growth stages.

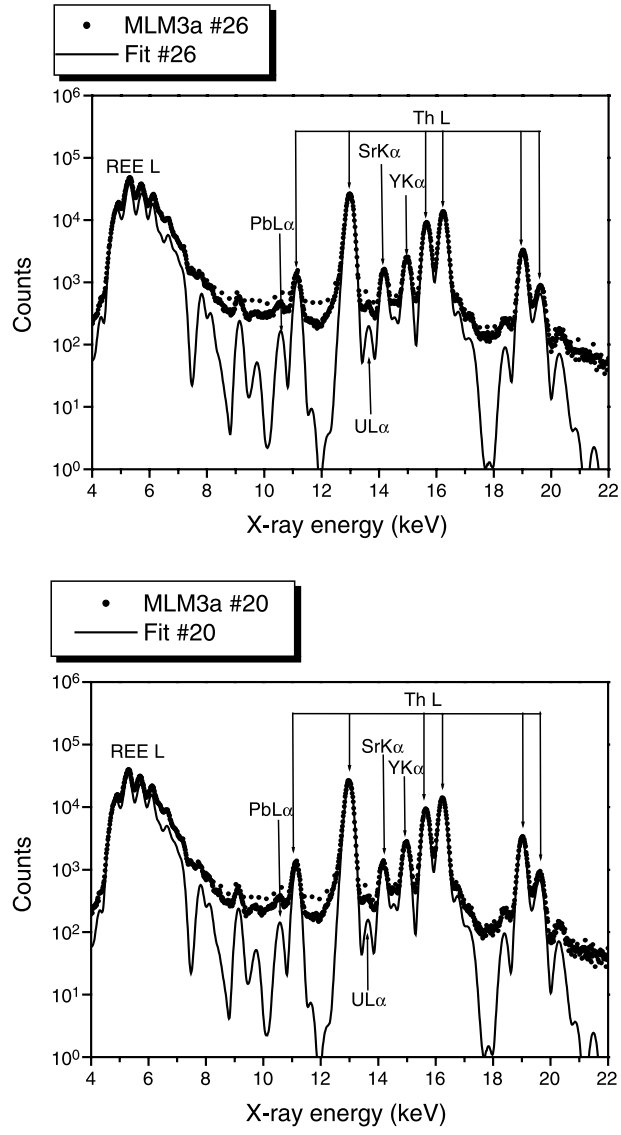

Fig. 2. GUPIX-reduced micro-PIXE spectra for two spot analyses of MLM3A monazite. The quantified concentrations are reported in Table 2

Table 2. Micro-PIXE data of two selected sub-zones on MLM3A monazite

Elem sub-zone 7	Conc. [ppm]	MDL (minimum detection limit) [ppm]	Elem sub-zone 2	Conc. [ppm]	MDL (minimum detection limit) [ppm]
Sr	1170 ± 3%	25	Sr	2450 ± 3%	25
Y	3570 ± 2%	90	Y	2230 ± 2%	90
Pb	160 ± 20%	60	Pb	180 ± 20%	60
Th	92300 ± 1%	80	Th	66200 ± 1%	80
U	1110 ± 6%	100	U	720 ± 6%	100
Calculated age (Ma)	37 ± 7		Calculated age (Ma)	60 ± 10	

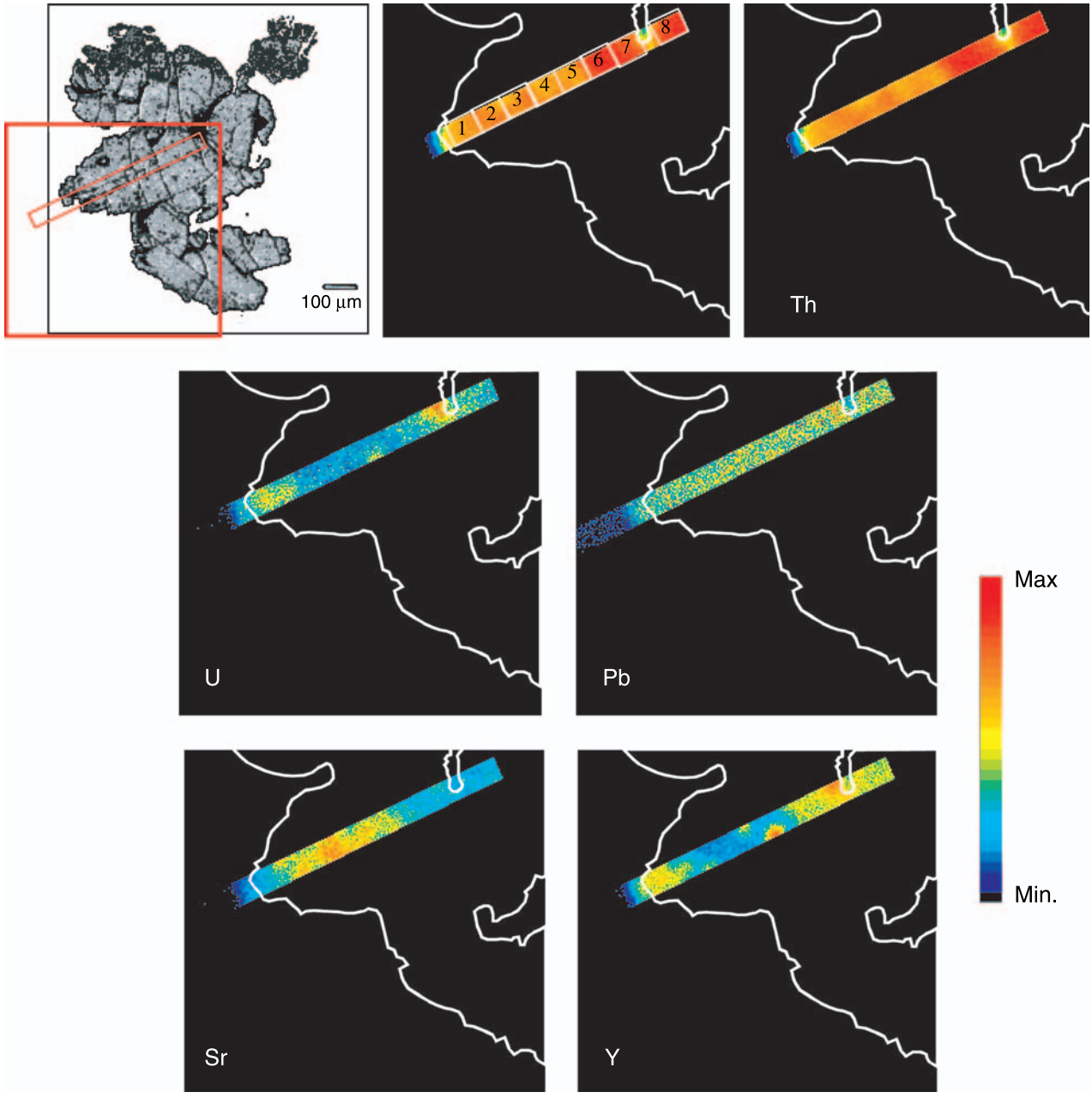

Fig. 3. Maps collected with a "*Full 256 × 256 raster*" scan on the sample area (~750 × 750 µm^2) indicated with a red square on the crystal image obtained with the electron microscope. The white lines on the maps represent the crystal borders of MLM3A monazite and the 8 subzones in the analysed PIXE stripe

Micro-PIXE data have been collected as single spot analyses on the higher-Th cheralite phase and on the lower-Th (Ce)-monazite, and as area maps along portions with the largest variation of Th contents. Two representative spectra of the BIG detector obtained from two spot analyses of $\sim 100 \times 100$ µm are reported in Fig. 2 whereas the Th, U, Pb Y and Sr data corresponding to the same analysed areas are reported in Table 2.

Figure 3 shows the micro-PIXE Th map of sample MLM3A, that was used to select a stripe (550 µm long) to be quantitatively analysed. Maps of elements of interest, obtained from scanning the stripe are also reported. This stripe was later on divided into 8 subzones (each 60–70 µm long) numbered starting from left side to right side in order to obtain a concentration profile. The portion external to the crystal as well as the portion with an intervening fracture were excluded. Figure 4 shows Pb, U, Th, Sr and Y concentration profiles obtained plotting concentrations measured in the 8 sub-zones. The zoning effect for Th, U, Sr and Y is evident, as well as the anti-correlated behaviour of Sr and Y.

Weight concentrations of U, Th and Pb by micro-PIXE analysis were used as input data for age determination using the equilibrium formula of [2, 3]. This formula contains the weight fractions of Pb, U and Th as measured by micro-PIXE, the corresponding isotopic atomic weights, abundance of the two U isotopes and the radioactive decay constants for both U isotopes and Th. Errors in determining concentrations of Pb, Th and U are estimated by the GUPIX software

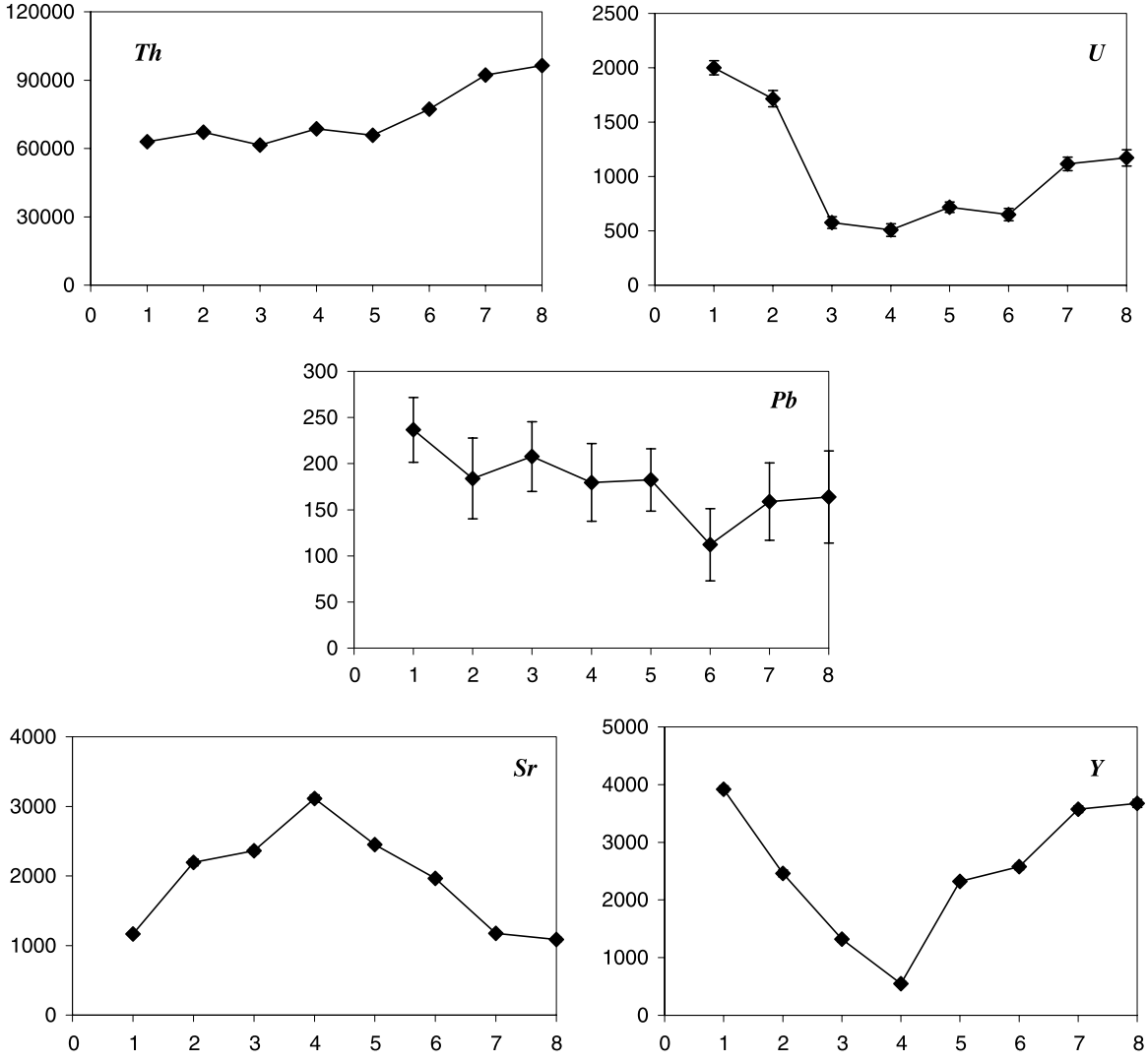

Fig. 4. Th, U, Pb, Sr and Y concentration profiles obtained on the 8 sub-zones selected on the PIXE stripe

and the age error was estimated calculating the propagating errors, resulting around 15% for single spot analyses, but in higher errors for age maps.

Two main age groups for monazite growth were calculated (Table 2). The younger age group of *ca.* 35 Ma, resulting from higher-Th areas, records the thermal peak of the UHP metamorphic event, in agreement with Th–Pb and U–Pb isotopic ages of 32–34 Ma measured by [13] on monazite from the fine-grained pyrope whiteschist of the classical Case Ramello (Parigi) outcrop.

An older age of *ca.* 60 Ma, resulting from monazite areas with lower Th concentrations, possibly records metamorphic growth during subduction of the UHP unit, but has to be confirmed by U–Th–Pb isotopic data on a larger sample set of monazite inclusions, as it could also result from Pb contamination (J. Hermann pers. com., 2005).

Conclusions

1) *In situ* microchemical analyses of monazite inclusions in pyrope megablasts of whiteschist from the UHP Brossasco-Isasca Unit of the Dora-Maira Massif indicate Ce- and Th-rich compositions, with Th contents ranging from about 7 wt.% to nearly 11 wt.%.
2) Variations in Th concentration are accompanied by an increase of some minor elements such as Ca and Sr and by changes in concentration of some of the LREE (Ce_2O_3: $26 \div 30$ wt.%; La_2O_3: $10.5 \div 13.5$ wt.%; Nd_2O_3: $10.5 \div 12$ wt.%).
3) Concentrations of Th, U and Pb obtained by micro-PIXE analysis were used as input data for age determination using the equilibrium formula of [2, 3], An age of *c.* 35 Ma was found in high-Th monazite areas, while an age of *c.* 60 Ma was found in low-Th areas.
4) Th–U–Pb age data suggest two monazite growth events. While the younger age of 35 Ma corresponds to the thermal and baric peak of the UHP metamorphism in the Brossasco-Isasca Unit, in agreement with previous literature data, the older age of 60 Ma found in low-Th areas possibly represents a prograde metamorphic event during burial of this unit, but has to be confirmed by U–Th–Pb isotopic data.

Acknowledgements. This work was financially supported by Consiglio Nazionale delle Ricerche (C.N.R.), Istituto di Geoscienze e Georisorse: projects 2004–2005. Special thanks are extended to P. A. Mando' (University of Firenze) for providing access to the micro-PIXE facilities. Reviewers' comments helped improve the manuscript and are gratefully acknowledged.

References

[1] Williams M L, Jercinovic M J (2002) J Structural Geol 24: 1013
[2] Suzuki K, Adachi M (1991) J Geochem 25: 357
[3] Montel J M, Foret S, Veschambre M, Nicollet C, Provost A (1996) Chem Geol 131: 31
[4] Suzuki K, Adachi M (1994) Tectonophysics 235: 277
[5] Lekki J, Lebed S, Paszkowski M L, Kusiak M, Vogt J, Hajduk R, Polak W, Potempa A, Stachura Z, Styczen J (2003) Nucl Instr Meth 210: 472
[6] Mazzoli C, Hanchar J M, Della Mea G, Donovan J J, Stern R A (2002) Nucl Instr Meth 189: 394
[7] Compagnoni R, Hirajima T, Chopin C (1995) In: Coleman R G, Wang X (eds) Ultrahigh pressure metamorphism. Cambridge Univ. Press, New York, p 206
[8] Schertl H P, Schreyer W (1996) In: Basu A, Hart S (eds) Reading the isotopic code, Geophysical Monographs, 95, Washington, DC, Am Geophys Union, p 331
[9] Jarosewich E, Boatner L A (1991) Geostandards Newlett 15: 397
[10] Maxwell J A, Campbell J L, Teesdale W J (1989) Nucl Instr Meth 43: 218
[11] Maxwell J A, Teesdale W J, Campbell J L (1994) Nucl Instr Meth 95: 407
[12] Foster H J (1998) Am Mineral 83: 259
[13] Tilton G R, Schreyer W, Schertl H P (1991) Contrib Mineral Petrol 108: 22